Influence of Extreme Ultraviolet Irradiance Variations on the Precipitating Ion Flux From MAVEN Observations

Antoine Martinez, François Leblanc, Jean-Yves Chaufray, Ronan Modolo, Olivier Witasse, Y. Dong, T. Hara, J. Halekas, R. Lillis, J. Mcfadden, et al.

Influence of Extreme Ultraviolet irradiance variations on the precipitating ion flux from MAVEN observations.

A. Martinez [1], F. Leblanc[1], J. Y. Chaufray [1,2], R. Modolo[2], O. Witasse[3], Y. Dong[4], T. Hara[5], J. Halekas[6], R. Lillis[5], J. McFadden[5], F. Eparvier[6], L. Leclercq[7], J. Luhmann[5], S. Curry[5], D. Titov[3] and B. Jakosky[6].

[1] LATMOS/IPSL Sorbonne Université, UVSQ, CNRS, Paris, France

[2] LATMOS/IPSL, UVSQ Université Paris-Saclay, Sorbonne Université, CNRS, Guyancourt, France

[3]ESTEC, European Space Agency, Noordwijk, Netherlands

[4] Laboratory for Atmospheric and Space Physics, University of Colorado, Boulder, CO, USA

[5] Space Science Laboratory, University of California, Berkeley, CA, USA

[6] Department of Physics and Astronomy, University of Iowa, IA, USA

[7] University of Virginia, Charlottesville, VA 22904, USA.

Abstract:

We study the influence of the solar EUV flux intensity on the precipitating ion fluxes as seen by MAVEN/SWIA, an energy and angular ion spectrometer. We defined three periods with significantly different EUV flux intensity (1.6 and 3.2 times the lowest EUV intensity) and compare the precipitating ion flux measured by MAVEN/SWIA during each period. At low energy [30-650] eV, we find that the median (average) precipitating ion flux during the medium and low EUV periods are respectively 1.7 (2.1) and 3 (3.5) times more intense than the flux during the high EUV period. At high energy [650-25000] eV, a similar trend in the intensity of the precipitating ion flux is observed but with an increase by 50% (46%) and 70% (79%) respectively. A larger EUV flux does therefore not seem to favour heavy ion precipitation into Mars' atmosphere, contrary to modelling prediction and overall expectations.

I. Introduction

Mars' upper atmosphere is constantly bombarded by energetic ions from either the solar wind or from Mars' exosphere (planetary pickup ions) (Lillis et al. 2015). Planetary ions created by the ionization of exospheric neutral particles can be accelerated by the motional solar wind electric field. Some of these ions escape (Brain et al. 2016), but a significant portion can impact Mars' atmosphere, leading to collisional cascade in Mars' thermosphere and to the ejection of atmospheric particles into the exosphere (Luhmann and Kozyra, 1991). This process, named "atmospheric sputtering" (Johnson, 1994), could have induced a significant atmospheric loss along Mars' history (Luhmann et al., 1992; Leblanc, and Johnson, 2001 and 2002).

Atmospheric escape induced by sputtering at present epoch is expected to be small compared to other mechanisms (Leblanc et al. 2017) and so difficult to measure. However, since the main driver of sputtering is ion precipitation (Johnson et al, 2000; Wang et al, 2014;2015), it is crucial to constrain the dependence of the precipitating ion flux on present solar wind conditions. While many studies have been carried out on the influence of the Extreme-Ultraviolet/Ultraviolet (EUV/UV) flux on the Martian environment as well as on ion escape (Modolo et al., 2005; Ma and Nagy, 2007; Terada et al. 2009; Edberg et al., 2009; Lundin et al, 2008,2013; Ramstad et al., 2015; Dong et al., 2017), the relation between ion precipitation and EUV flux has only been studied in theoretical works (Chaufray et al., 2007; Leblanc and Johnson, 2002; Wang et al., 2014,2015) and briefly discussed in Nilsson et al., 2012. We therefore describe here the first empirical study on the influence of the EUV flux on ion precipitation by analyzing MAVEN measurements (Jakosky et al. 2015). In section II, we describe the set of data used in this work. In section III, we carefully analyzed the various potential solar wind drivers to extract three sets of measurements obtained during different EUV flux intensity but for similar solar wind conditions and geographical coverage. In section IV, we summarize and discuss the main results of this study and conclude in section V.

II. Data set used for this analysis

We use measurements performed by the Solar Wind Ion Analyzer (SWIA) (Halekas et al., 2015), the Magnetometer (MAG) (Connerney et al., 2015a; 2015b) and the Solar Extreme Ultraviolet Monitor (EUVM) (Eparvier et al., 2015). The MAVEN/SWIA is an energy and angular ion spectrometer covering an energy range between 25eV/q and 25keV/q with 48 energy steps logarithmically spaced, a field of view (FOV) of 360°x90° on 64 angular bins and 4s time resolution. We based our study on MAVEN/SWIA despite the lack of mass resolution because MAVEN/STATIC (which has mass resolution) has much more restricted coverage of the precipitating flux. The MAVEN/EUVM measures the solar irradiance in three bands from the soft X-ray to the EUV range (in three spectral bands 0.1-7nm, 17-22nm and 121-122nm) with a temporal resolution of 1s. The solar wind density, speed, and IMF vector are measured by MAVEN/SWIA and MAVEN/MAG and averaged on an orbit-by-orbit basis in order to characterize the solar wind conditions (Halekas et al., 2017). We then reconstruct the Mars Solar Electric (MSE) coordinate system in which the X-axis is toward the Sun, the Z-axis points along the solar wind motional electric field and the Y-axis completing the right hand system (Fedorov et al., 2006).

In order to reconstruct the precipitating ion flux, we follow the method described in Leblanc et al. (2015) and Martinez et al (2019). We select all MAVEN measurements performed between 200 and 350km. Within such altitude range, any ion which velocity direction is at less than 75° with respect to the local nadir direction has a very large probability to impact Mars' atmosphere. Therefore, to reconstruct the precipitating flux, we sum all measurements of SWIA anodes which FOV is at less than 75° from the local zenith direction. Moreover, in order to exclude reconstructed precipitating flux with poor coverage, we only consider measurements during which the total FOV of SWIA anodes is more than 65% of the 75° solid angle cone centered on the zenith direction.

In this study, to characterize the EUV flux during the declining solar cycle from medium to minimum activity, we use the MAVEN/EUVM channel A which measures solar irradiance between 17 and

22nm. We sort the MAVEN data from December 2014 to July 2018 into three periods: high EUV (From 2 December 2014 to 10 March 2015) with an average EUV flux of 0.42mW.m^{-2}, medium EUV (From 4 June 2015 to 22 October 2015, from 23 December 2015 to 1 June 2016, and from 4 December 2016 to 20 July 2017) with an average EUV flux of 0.21mW.m^{-2} and low EUV (from 28 November 2017 to 31 July 2018) with an average EUV flux of 0.13mW.m^{-2}. These three intervals represent several different Mars seasons. Table 1 summarizes the main characteristics of each period.

	High	**Medium**	**Low**
[Date begin-Date End] (dd/mm/yyyy)	[02/12/2014-10/03/2015]	[04/06/2015-22/10/2015] [23/12/2015-01/06/2016] [04/12/2016-30/07/2017]	[28/11/2017 31/07/2018]
Heliocentric distance (AU)	[1.38-1.43]	[1.54-1.66] [1.49-1.66] [1.39-1.63]	[1.40-1.65]
Solar Longitude (LS) °	[244.3°-305.2°] (northern hemisphere winter)	[352.5°-57.9°] [85.1°-161.5°] [273.5°-35.7°] (one Martian year)	[93.4°-221.1°] (northern hemisphere summer and autumn)
Mean EUV flux $(mW.m^{-2})$ from channel A of MAVEN/EUVM	0.42	0.21	0.13
Average Precipitating ion flux $(eV.cm^{-2}.sr^{-1}.s^{-1})$ [30,650] eV	$1.18\ (\pm 0.11) \times 10^7$	$2.49\ (\pm 0.12) \times 10^7$	$4.05\ (\pm 0.33) \times 10^7$
Median Precipitating ion flux $(eV.cm^{-2}.sr^{-1}.s^{-1})$ [30,650] eV	0.62×10^7	1.07×10^7	1.83×10^7
Average Precipitating ion flux $(eV.cm^{-2}.sr^{-1}s^{-1})$ [650,25000] eV	$15.9\ (\pm 0.7) \times 10^7$	$23.9\ (\pm 0.7) \times 10^7$	$26.9\ (\pm 1.1) \times 10^7$
Median Precipitating ion flux $(eV.cm^{-2}.sr^{-1}s^{-1})$ [650,25000] eV	11.0×10^7	16.1×10^7	19.7×10^7
Number of measurements	425	1205	374

Table 1: *Summary of each period of our study. In brackets, the 1-sigma standard deviation (uncertainty) of the precipitating ion flux values.*

III. Upstream solar wind conditions and planetary coverage

To investigate the Solar EUV dependence of the precipitating ion flux, we first need to reconstruct the solar wind parameters. Lillis et al. (2015), Edberg et al. (2009) and Ramstad et al., (2017) suggested that the dynamic pressure compresses Mars' magnetosphere and favors the acceleration and precipitation of the planetary pickup ions. Martinez et al. (2019) and Hara et al. (2017a) showed that the precipitating ion flux can be organized with respect to the orientation of the solar wind convective electric field. Also, the presence of crustal magnetic fields (Acuña et al., 1999; Connerney et al., 2005) can also influence locally the precipitating ion flux, as shown by Hara et al. (2017b). For each orbit, during which the precipitating flux was measured, we therefore used the part of MAVEN orbit in the solar wind to infer the solar wind. We use such solar wind measurements prior to our precipitating flux measurement if the time difference between the two measurements is less than 4 hours and 30 minutes (the MAVEN orbital period). We assume that the solar wind conditions do not change significantly between MAVEN measurements of the solar wind and MAVEN measurements of the precipitating flux (in average 2 hours and 20 minutes).

In order to verify the validity of this assumption, we compare the solar wind density and speed measurements from Mars Express(MEX)/ASPERA-3 (Barabash et al., 2006) with those measured by MAVEN. Starting from $n_{MAVEN/SW}\ and\ V_{MAVEN/SW}$ the solar wind density and speed as measured by MAVEN/SWIA before a measurement of the precipitating flux below 350 km, we determine $n_{MEX/SW}\ and\ V_{MEX/SW}$, as measured by MEX/ASPERA-3 (Barabash et al., 2006) when MAVEN's altitude was within the time interval during which SWIA measured the precipitating flux. We only consider ASPERA-3 measurements if the measured density was larger than 0.01cm^{-3} and the quality flag larger than 0.6.

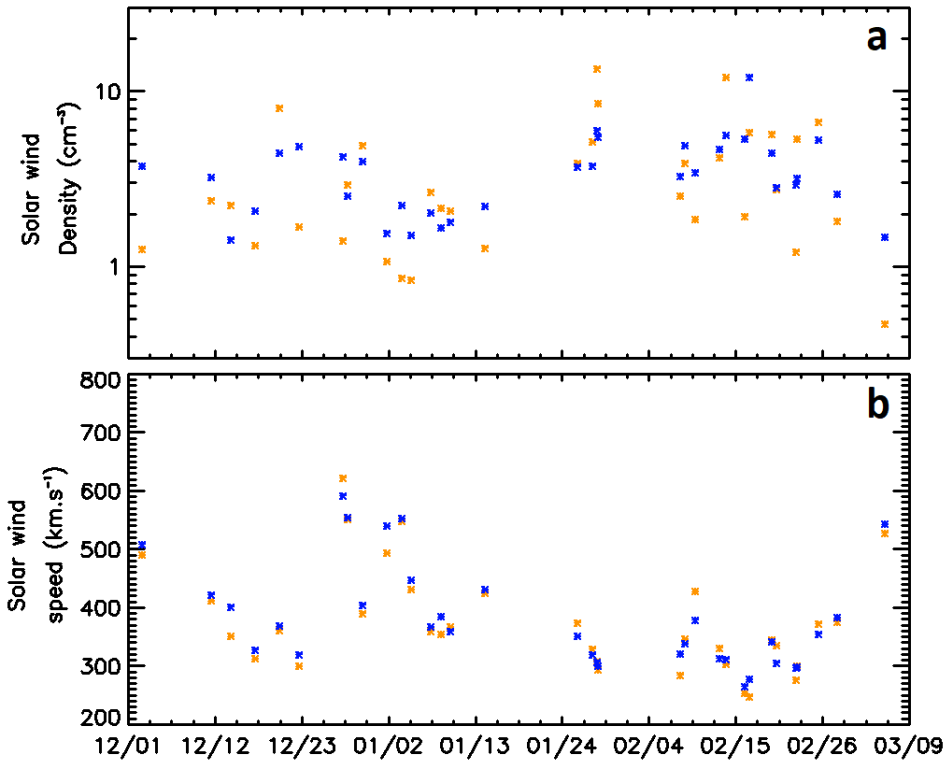

126

127 *Figure 1: Comparison between the measured solar wind parameters by MAVEN/SWIA (blue) and*
128 *MEX/ASPERA-3 (orange) for the high EUV period (from December 2014 to March 2015):* ***(a)*** *the*
129 *solar wind density,* ***(b)*** *Solar wind speed.*

130 With such criteria, we did not identify any measurement for the low EUV period and ASPERA-3
131 measurements for 4.2% and 8.0% of MAVEN precipitating flux measurements for the medium and
132 high EUV periods (see also the supplementary materials, Table S.1). The set of measurement
133 comparisons displayed in Figure 1 for the high EUV period, show that the solar wind speeds as
134 measured by SWIA and ASPERA-3 are usually in very good agreement (MAVEN: 403 ± 12km/s and
135 MEX: 396 ± 12km/s, for 85 measurements). Contrary to the solar wind speed, the measurements of
136 the density display a relatively poor agreement (Figure 1b) but still acceptable in an average and
137 within the one-sigma dispersion (MAVEN: $3.31 \pm 0.35 cm^{-3}$ and MEX: $3.07 \pm 0.31 cm^{-3}$, for 85
138 measurements).
139 The approach to select the set of measurements used for our study follows the method developed in
140 Dong et al. (2017). As in Dong et al. (2017), we restrict the set of precipitating measurements to

those obtained during solar wind conditions with dynamic pressure $P_{dyn} = m_p n_{SW} V_{SW}^2$, (where m_p is the mass of the proton, n_{SW} and V_{sw} the solar wind density and velocity) between 0.3 and 2.6nPa (moderate solar wind dynamic pressure) and with IMF strength between 2.2 and 6.7nT. We also restrict our sample of precipitation measurements to those obtained in an SZA interval between 70° and 130°. Furthermore, in order to avoid the potential influence of the crustal fields (Leblanc et al. 2017; Hara et al. 2017b), we also only consider measurements performed when the average magnetic field between 200 and 350km is less than 60nT. For each set of solar wind parameters, we calculate the solar wind dynamic pressure, the norm of the solar wind motional electric field defined as $E = \left|\vec{V}_{SW} \times \vec{B}_{IMF}\right|$ where B_{IMF} is the interplanetary magnetic field (IMF), the Alfvén Mach number $M_A = V_{SW}/V_A$ where V_A is the Alfvén speed, the solar wind flux defined as $F_{SW} = n_{SW} V_{sw}$ and the pickup O^+ gyroradius in the solar wind $R_g = \frac{m_O V_{SW} \sin\theta_{cone}}{q B_{IMF}}$ where m_O is the mass of an O^+ ion, θ_{cone} is the angle between the IMF direction and the MSO X-axis and q is the electron charge value. We also define the MSE angle as the anticlockwise angle between the vector formed by the latitude and the longitude in MSE of the position where the ion precipitation is being measured and the East MSE direction (MSE longitude equal to +180° and latitude equal to 0°) (Martinez et al., 2019).

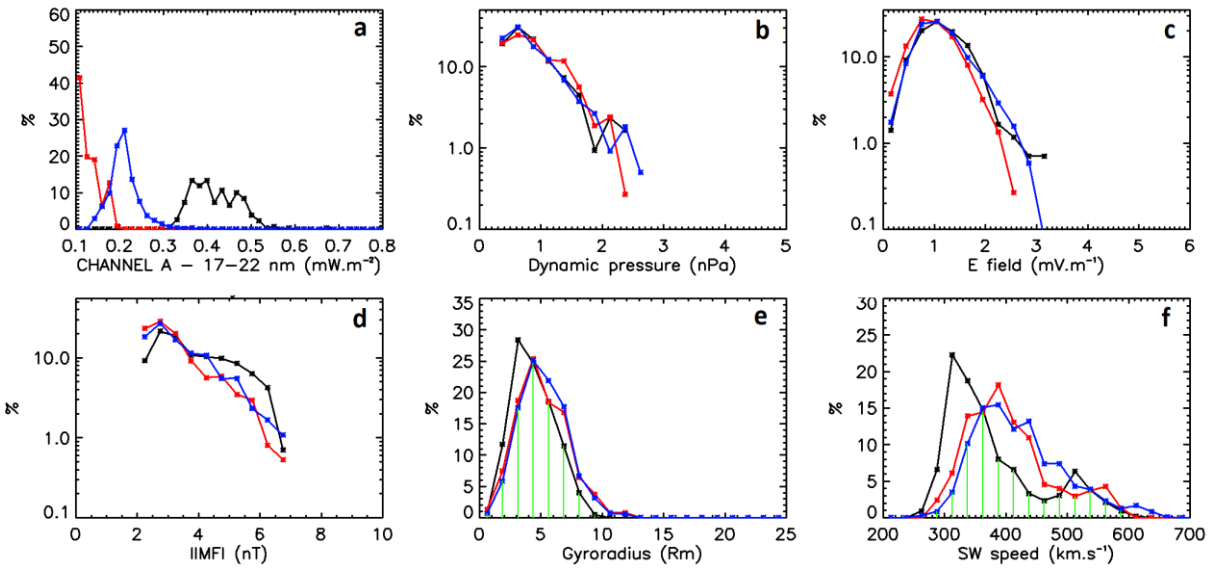

Figure 2: Distribution of the set of measured solar wind parameters for the high EUV period (black), the medium EUV period (dark blue) and the low EUV period (red): ***(a)*** *Values of the EUV photon flux as measured by MAVEN/EUVM instrument,* ***(b)*** *Solar wind dynamic pressure,* ***(c)*** *Solar wind convective electric field,* ***(d)*** *Interplanetary Magnetic Field as measured by MAVEN/MAG,* ***(e)*** *pickup O^+ ion gyroradius calculated in the solar wind and* ***(f)*** *solar wind speed determined by MAVEN/SWIA. The green zone in 2.e and 2.f correspond to the portion of the distribution common to the three periods.*

In order to demonstrate that the selected sets of measurement for the three EUV periods are similar in terms of solar wind conditions and planetary geographic coverage (MSO and MSE frames, see also the supplementary materials, Figures S.1 and S.2), we calculate for each parameter, the area (green part in Figure 2.e and 2.f) common to the three distributions. The ratio between this common area and each of the three areas provides a measure of the overlap between the three sets of measurement for a given solar wind parameter. In Table 2, for 10 solar parameters, we provide the minimum percentage of the distribution areas in common to the three periods as well as the first and third quartile, the mean and 1-sigma standard deviation of each parameter.

Figure 2 displays the distribution of the values of each of these parameters for the three EUV periods and illustrates our method to determine the similarity between these sets of measurement. As an example, in the case of the gyroradius (Figure 2.e), at least 83% of each sets of measurement were performed for similar values of this parameter. This percentage decreases to 62% for the solar wind speed (Figure 2.f). On the other hand, the three EUV periods are clearly distinct (Figure 2.a) and correspond to a null common area (Table 2).

		High	**Medium**	**Low**	**Common coverage (%)**
EUV Flux	$\mu \pm \sigma$	0.42 ± 0.08	0.21 ± 0.04	0.13 ± 0.02	0.0

$mW.m^{-2}$	Q25	0.37	0.19	0.11	
	Q75	0.46	0.22	0.14	
Dynamic pressure nPa	$\mu \pm \sigma$	0.87 ± 0.44	0.85 ± 0.46	0.90 ± 0.43	86.0
	Q25	0.56	0.52	0.56	
	Q75	1.08	1.05	1.14	
Electric field $mV.m^{-1}$	$\mu \pm \sigma$	1.18 ± 0.50	1.15 ± 0.51	1.00 ± 0.43	85.4
	Q25	0.83	0.80	0.74	
	Q75	1.48	1.42	1.27	
IMF nT	$\mu \pm \sigma$	3.84 ± 1.16	3.43 ± 1.04	3.25 ± 0.98	74.5
	Q25	2.89	2.59	2.52	
	Q75	4.74	4.06	3.67	
Gyroradius R_g R_{Mars}	$\mu \pm \sigma$	4.36 ± 1.72	5.22 ± 1.94	5.08 ± 2.02	83.2
	Q25	2.87	3.80	3.61	
	Q75	5.51	6.54	6.41	
Alfvén Mach number	$\mu \pm \sigma$	8.89 ± 2.71	9.68 ± 2.71	10.6 ± 3.0	74.2
	Q25	6.87	7.88	8.40	
	Q75	10.1	11.3	12.3	
Speed $km.s^{-1}$	$\mu \pm \sigma$	378 ± 78	422 ± 74	406 ± 70	61.6
	Q25	317	369	353	
	Q75	413	464	443	
Density cm^{-3}	$\mu \pm \sigma$	4.00 ± 2.60	3.02 ± 1.86	3.63 ± 2.25	76.5
	Q25	2.21	1.67	1.89	
	Q75	4.89	3.70	4.99	
Angle MSE (°)	$\mu \pm \sigma$	185 ± 112	202 ± 111	172 ± 115	67.1
	Q25	143	149	38.8	
	Q75	306	326	208	
Solar wind flux $10^8\ s^{-1}cm^{-2}$	$\mu \pm \sigma$	1.42 ± 0.77	1.21 ± 0.67	1.38 ± 0.73	79.0
	Q25	0.88	0.72	0.81	
	Q75	1.70	1.50	1.80	

Table 2: *Mean μ, standard deviation σ, first quartile Q25 and third quartile Q75 of each solar parameter distribution for the three sets of precipitating flux measurement. The last column provides the percentage of the area in common between the 3 distributions.*

If we now only consider the medium and low periods, for all parameters listed in Table 2, the distribution area in common to these two sets of measurement represents more than 75% of each distribution. According to these percentages, we conclude that the three sets of precipitating ion measurements were obtained under similar solar wind conditions.

To further demonstrate this conclusion, considering the solar wind speed parameter with the less similar distributions between the three periods, we reduce each sample so that the solar wind speed measured during each period was restricted to values between 370 and 500km/s. In that case, the percentage increases to 81%. We then calculate the values of the precipitating ion flux with these

reduced samples (see also the supplementary material, Table S.2) and found that all measured precipitating flux values are equivalent for the two different samples except during the medium period when the flux values differ slightly more than one sigma. In another words, the reduction of the sampling improves the similarity between the three sets of measurement and does not change significantly the measured precipitating ion flux

IV. Results and Analysis

Our results show that the average ion precipitation decreases when the EUV flux increases (see Table 1 and Figure 3). The energy dependence of the differential flux is similar from one period to the other, but we can note that the increase in precipitating ion flux is more significant for energies below 1 to 3 keV than above. This conclusion is not consistent with studies modelling the precipitating ion flux for different solar EUV fluxes (Chaufray et al., 2007) which showed that the flux of O^+ which re-impacts the atmosphere should be smaller at solar minimum than at solar maximum. However, they also concluded that the differences between the two periods were smaller than predicted by Luhmann et al. (1992) using simple gas dynamic description of Mars' interaction with the solar wind. These authors explained this difference by the deceleration of the solar wind due to the mass-loading (Dubinin and Lundin, 1995) which happens further away from Mars at high solar activity and reduces therefore the probability of accelerated pickup ions to re-impact Mars' atmosphere.

Mass-loading depends to first order on the ionization rate of the Martian exosphere. The exospheric density at a given altitude also depends on the EUV/UV flux which heats the Martian thermosphere whereas the ionization rate directly depends on the solar radiation flux in the wavelength range below 91nm. Forbes et al. (2008) found a very good correlation (0.96) between the long-term EUV flux (proxy F10.7) and the Martian exospheric density at 390km in altitude. Seasonal variations of the exosphere might also significantly impact the density at a given altitude as studied in Bhattacharyya

et al, (2015) and Chaufray et al, (2015), as well as the position of the bow shock (Halekas et al, 2017). A peak of exospheric hydrogen density during the Martian dust season was reported by Chaffin et al. (2014), Bhattacharyya et al, (2015) and Halekas (2017) between Ls=200° and 300°. Therefore, an increase in mass-loading of the solar wind might be related to this seasonal variability but would only explain the decrease of the precipitating flux during the high EUV period. During the low and medium periods, there are no significant change in season so that the difference in precipitating flux cannot be associated to seasonal variability.

As originally suggested by Johnson & Luhmann (1998), an increase of the EUV/UV flux should increase the number of pickup exospheric ions but might also load more efficiently the solar wind and reduce the percentage of these ions able to re-impact the atmosphere. What our study seems to suggest is that this effect might be much more efficient than shown in Chaufray et al. (2007), perhaps due to the limited spatial resolution of their simulation at this time (~300km).

Another potential effect is the MSO latitude of the crustal magnetic fields which is solar dependent. Brain et al. (2005) showed that the Magnetic Pile-Up Boundary altitude changes significantly with season because of the latitude variation of the main crustal field structure (centered at 180° GEO East longitude and -50° GEO latitude) along one Martian year. Such effect might be actually due to an increase exospheric hydrogen density rather due to the crustal fields latitudes according to Chaufray et al. (2015). Actually, Hall et al. (2016) shows that an increase in the EUV flux is associated with a position of the bow shock further from Mars, suggesting also an influence of the exosphere on the induced magnetosphere. In any case, we cannot exclude that part of the variation in precipitating flux described here might be due to the crustal field, as actually shown by Hara et al. (2017b). We calculate the average position of the main crustal field structure for the three sets of measurements and found $-47 \pm 17°$, $-45 \pm 16°$, and $-46 \pm 17°$ latitude MSO and $27 \pm 106°$, $-20 \pm 107°$ and $-3 \pm 84°$ longitude MSO for the low, medium and high EUV periods. Therefore, the relative variation of the precipitating ion flux between the three periods selected in our paper might be also related to the variation of the crustal field latitudinal positions. In order to test this possibility, we further

reduce our set of measurements in order to only use measurements of the precipitating ion flux performed when the main crustal field structure was at a SZA larger than 120°. The reconstructed differential precipitating ion fluxes display very similar relative variation showing, here again, that the main driver for this variation should be the EUV flux.

Dong et al. (2017) found that the total escape rate of oxygen ions with E_i≥6 eV increases by 1.5 when the EUV flux increases by a similar factor. Our analysis suggested that an increased EUV flux induces a decrease of the ion precipitation. In the case of the high EUV period (similar to that in Dong et al (2017)), for the ions with E_i≥25 eV, we have an integrated precipitating flux equal to $1.3 \times 10^{22}\ particles.s^{-1}$ which should be compared to the estimate by Dong et al. (2017) of an escape rate of $1.8 \times 10^{24}\ particles.s^{-1}$ at $0.2\mathrm{R}_{\mathrm{Mars}}$ in altitude. Therefore, the precipitating flux represents only 1% of the escaping flux in the energy range considered in this paper.

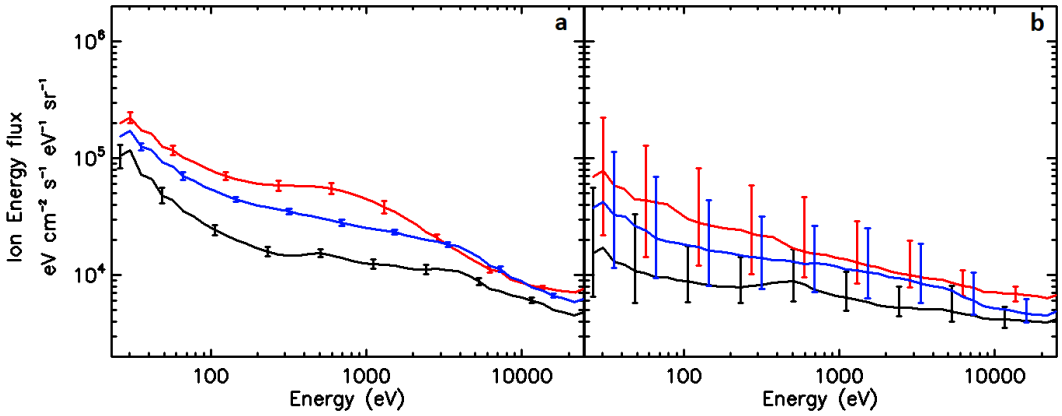

Figure 3: *Precipitating ion differential energy spectra as measured by MAVEN/SWIA during high EUV (black), medium EUV (dark blue) and low EUV periods (red):* ***(a)*** *Average value (with 1-sigma standard deviation) and* ***(b)*** *Median value (with first and third quarter).*

V. Summary and Conclusion

We study the precipitating ion flux from MAVEN instruments over more than three years of data divided into three intervals of solar EUV/UV intensity: between 2 December 2014 and 10 March 2015 (Ls from 244.3° to 305.2°), between 4 June 2015 and 1 June 2017 (two Ls periods: from 273.5° to 57.9° and from 85.1° to 161.5°) and between 28 November 2017 and 31 July 2018 (Ls from 93.4° to 221.1°). By constraining the solar wind conditions, we show that these three samples were obtained under similar solar wind conditions and cover similar regions in a MSE frame.

We reconstruct the measured precipitating ion flux by MAVEN/SWIA. The increase of the EUV flux intensity from 0.13 to 0.42mW.m^{-2} is clearly associated with a decrease of the precipitating ion flux from 18.3 to $6.2 \times 10^6 \mathrm{eV.cm^{-2}.sr^{-1}.s^{-1}}$ (by almost a factor 3) for the energy range between 30 and 650 eV and a decrease by 18% to 44% at higher energies ([650-25000] eV).

This somewhat surprising result, in contradiction with previous theoretical studies (Chaufray et al., 2007), might illustrate the complex relation between the variations of the exosphere as induced by the solar EUV/UV flux and the solar wind interaction with Mars. Dong et al. (2017) reported an almost linear dependence of the ion escape on the EUV/UV flux, whereas we have found an almost linear anti-correlation between the EUV flux and the precipitating ion flux. In others words, even if the EUV flux increase the ionization rate in the exosphere, the probability of a pickup ion to escape or to precipitate into the atmosphere should also be changed, illustrating a much more complex dependence of the fate of Mars' planetary ions on the solar conditions than anticipated.

Acknowledgements

This work was supported by the DIM ACAV and the ESA/ESTEC faculty. This work was also supported by CNES "Système Solaire" program and by the "Programme National de Planétologie" and "Programme National Soleil-Terre". This work is also part of HELIOSARES Project supported by the ANR (ANR-09-BLAN-0223), ANR MARMITE (ANR-13-BS05-0012-02) and ANR TEMPETE (ANR-17-CE31-

0016). Data analysis was performed with the AMDA science analysis system provided by the Centre de Données de la Physique des Plasmas (CDPP) supported by CNRS, CNES, Observatoire de Paris and Université Paul Sabatier, Toulouse. All data used in this paper are archived and available in the Planetary Data System Archive.

References

Acuña, M. H., et al. (1999), Global distribution of crustal magnetization discovered by the Mars Global Surveyor MAG/ER Experiment, *Science*, *284*, 790-793, doi:10.1126/science.284.5415.790.

Barabash, S., Lundin, R., Andersson, H. et al. Space Sci Rev (2006) 126: 113. https://doi.org/10.1007/s11214-006-9124-8

Bhattacharyya, D., Clarke, J. T., Bertaux, J.-L., Chaufray, J.-Y., and Mayyasi, M. (2015), A strong seasonal dependence in the Martian hydrogen exosphere, Geophys. Res. Lett., 42, 8678– 8685, doi:10.1002/2015GL065804.

Brain D. A., J. S. Halekas, R. Lillis, D. L. Mitchell, and R. P. Lin, Variability of the altitude of the Martian sheath, Geophys. Res. Let., 32, L18203, doi:10.1029/2005GL023126, 2005

Brain, D. A., F. Bagenal, Y.-J. Ma, H. Nilsson, and G. Stenberg Wieser (2016), Atmospheric escape from unmagnetized bodies, J. Geophys. Res. Planets, 121, 2364–2385, doi:10.1002/2016JE005162

Chaffin, M. S., Chaufray, J.-Y., Stewart, I., Montmessin, F., Schneider, N. M., and Bertaux, J.-L. (2014), Unexpected variability of Martian hydrogen escape, Geophys. Res. Lett., 41, 314– 320, doi:10.1002/2013GL058578.

Chassefière, E., and F., Leblanc (2004), Mars atmospheric escape and evolution; interaction with the solar wind, Planet. Space Sci., 52, 1039-1058, doi: 10.1016/j.pss.2004.07.002

312 Chaufray, J. Y., R. Modolo, F. Leblanc, G. Chanteur, R. E. Johnson, and J. G. Luhmann (2007), Mars
313 solar wind interaction: Formation of the Martian corona and atmospheric loss to space, J. Geophys.
314 Res., 112, E09009, doi: 10.1029/2007JE002915.

315 J.-Y. Chaufray, F. Gonzalez-Galindo, F. Forget, M.A. Lopez-Valverde, F. Leblanc, R. Modolo, S. Hess
316 (2015), Variability of the hydrogen in the martian upper atmosphere as simulated by a 3D
317 atmosphere–exosphere coupling, Icarus, Volume 245, 2015, Pages 282-294, ISSN 0019-1035,
318 https://doi.org/10.1016/j.icarus.2014.08.038.

319 Connerney, J.E.P., Açuna, M.H., Ness, N.F., Kletetschka, G., Mitchell, D., Lin, R.P., & Reme, H. (2005).
320 Tectonic implications of Mars crustal magnetism. Proc. Nat. Acad. Sci., Vol. 102, (42), 14970-14975,
321 doi: 10.1073/pnas.0507469102.

322 Connerney, J.E.P., Espley, J., Lawton, P. et al., The MAVEN Magnetic Field Investigation, Space Sci Rev
323 (2015a) 195 : 257., https://doi.org/10.1007/s11214-015-0169-4

324 Connerney, J.E.P., Espley, J.R., DiBraccio, G.A., et. al. (2015b). First results of the MAVEN magnetic
325 field investigation. Geophys. Res. Lett., 42, 8819–8827, doi:10.1002/2015GL065366.

326 Dong, Y., X. Fang, D. A. Brain, J. P. McFadden, J. S. Halekas, J. E. P. Connerney, F. Eparvier, L.
327 Andersson, D. Mitchell, and B. M. Jakosky (2017), Seasonal variability of Martian ion escape through
328 the plume and tail from MAVEN observations, *J. Geophys. Res. Space Physics*, 122, 4009–4022, doi:
329 10.1002/2016JA023517

330 Dubinin E., Lundin R., Mass-loading near Mars, Advances in Space Research, Volume 16, Issue 4,
331 1995, Pages 75-79, ISSN 0273-1177, https://doi.org/10.1016/0273-1177(95)00211-V.

332 Edberg, N., D. A. Brain, M. Lester, S. W. H. Cowley, R. Modolo, M. Franz, and S. Barabash (2009),
333 « Plamas boundary variability at Mars as observed by Mars Global Surveyor and Mars Express », Ann.
334 Geophys., 27, 3537-3550, doi:10.5194/angeo-27-3537-2009.

335 Eparvier, F.G., Chamberlin, P.C., Woods, T.N. et al., The Solar Extreme Ultraviolet Monitor for
336 MAVEN, Space Sci Rev (2015) 195 : 293., https://doi.org/10.1007/s11214-015-0195-2

337 Fang, X., S. W. Bougher, R. E. Johnson, J. G. Luhmann, Y. Ma, Y.-C. Wang, and M. W. Liemohn (2013),
338 The importance of pickup oxygen ion precipitation to the Mars upper atmosphere under extreme
339 solar wind conditions, *Geophys. Res. Lett.*, 40, 1922–1927, doi: 10.1002/grl.50415.

340 A. Fedorov, E. Budnik, J.-A. Sauvaud, C. Mazelle, S. Barabash, R. Lundin, M. Acuña, M. Holmström, A.
341 Grigoriev, M. Yamauchi, H. Andersson, J.-J. Thocaven, D. Winningham, R. Frahm, J.R. Sharber, J.
342 Scherrer, A.J. Coates, D.R. Linder, D.O. Kataria, E. Kallio, H. Koskinen, T. Säles, P. Riihelä, W. Schmidt,
343 J. Kozyra, J. Luhmann, E. Roelof, D. Williams, S. Livi, C.C. Curtis, K.C. Hsieh, B.R. Sandel, M. Grande, M.
344 Carter, S. McKenna-Lawler, S. Orsini, R. Cerulli-Irelli, M. Maggi, P. Wurz, P. Bochsler, N. Krupp, J.
345 Woch, M. Fränz, K. Asamura, C. Dierker, Structure of the Martian wake, Icarus, Volume 182, Issue 2,
346 2006, Pages 329-336, ISSN 0019-1035, https://doi.org/10.1016/j.icarus.2005.09.021.

347 Forbes, J. M., F. G. Lemoine, S. L. Bruinsma, M. D. Smith, and X. Zhang (2008), Solar flux variability of
348 Mars' exosphere densities and temperatures, *Geophys. Res. Lett.*, 35, L01201,
349 doi:10.1029/2007GL031904.

350 Halekas, J. S. (2017), Seasonal variability of the hydrogen exosphere of Mars, J. Geophys. Res.
351 Planets, 122, 901– 911, doi:10.1002/2017JE005306.

352 Halekas, J.S., Taylor, E.R., Dalton, G. et al., The Solar Wind Ion Analyzer for MAVEN, Space Sci Rev
353 (2015) 195 : 125., https://doi.org/10.1007/s11214-013-0029-z

354 Halekas, J. S., et al. (2017), Structure, dynamics, and seasonal variability of the Mars-solar wind
355 interaction: MAVEN Solar Wind Ion Analyzer in-flight performance and science results, *J. Geophys.*
356 *Res. Space Physics*, 122, 547–578, doi: 10.1002/2016JA023167.

Hall, B. E. S., et al. (2016), Annual variations in the Martian bow shock location as observed by the Mars Express mission, J. Geophys. Res. Space Physics, 121, 11,474–11,494, doi:10.1002/2016JA023316.

T. Hara, K. Seki, Y. Futaana, M. Yamauchi, M. Yagi, Y. Matsumoto, M. Tokumaru, A. Fedorov, and S. Barabash (2011), Heavy-ion flux enhancement in the vicinity of the Martian Ionosphere during CIR passage: Mars Express ASPERA-3 observations, JOURNAL OF GEOPHYSICAL RESEARCH, VOL. 116, A02309, doi:10.1029/2010JA015778, 2011

Hara, T., et al. (2017a), MAVEN observations on a hemispheric asymmetry of precipitating ions toward the Martian upper atmosphere according to the upstream solar wind electric field, J. Geophys. Res. Space Physics, 122, 1083–1101, doi: 10.1002/2016JA023348

Hara T. et al., (2017b), Evidence for crustal magnetic field control of ions precipitating into the upper atmosphere of Mars, J. Geophys. Res. Space Physics, 122, doi: 10.1029/2017JA024798.

Jakosky, B.M., Lin, R.P., Grebowsky, J.M. et al., The Mars Atmosphere and Volatile Evolution (MAVEN) Mission, Space Sci Rev (2015) 195 : 3. https://doi.org/10.1007/s11214-015-0139-x

Johnson, R.E., Plasma-induced sputtering of an atmosphere, Space Sci Rev (1994) 69: 215. https://doi.org/10.1007/BF02101697

Johnson, R. E., and J. G. Luhmann (1998), Sputter contribution to the atmospheric corona on Mars, *J. Geophys. Res.*, 103(E2), 3649–3653, doi: 10.1029/97JE03266.

Johnson, R. E., D. Schnellenberger, and M. C. Wong (2000), The sputtering of an oxygen thermosphere by energetic O^+, *J. Geophys. Res.*, 105(E1), 1659–1670, doi: 10.1029/1999JE001058

Leblanc, F. and R.E Johnson (2001), Sputtering of the Martian atmosphere by solar wind pick-up ions, *Planet. Space Sci*., 49, 645-656, 2001, doi:10.1016/S0032-0633(01)00003-4.

379 Leblanc F. and R.E. Johnson (2002), Role of molecules in pick-up ion sputtering of the Martian
380 atmosphere, *J. Geophys. Res.*, https://doi.org/10.1029/2000JE001473

381 Leblanc F., R. Modolo and al. (2015), Mars heavy ion precipitating flux as measured by Mars
382 Atmosphere and Volatile EvolutioN, Geophys. Res. Lett, 42, 9135-9141, doi: 10.1002/2015GL066170.

383 Leblanc F., Chaufray, J. Y., Modolo, R., Leclercq, L., Curry, S., Luhmann, J., … Jakosky, B. (2017). On the
384 origins of Mars' exospheric nonthermal oxygen component as observed by MAVEN and modeled by
385 HELIOSARES. Journal of Geophysical Research: Planets, 122, 2401–2428.
386 https://doi.org/10.1002/2017JE005336

387 Leblanc, F. and al., (2018). On Mars' Atmospheric Sputtering after MAVEN first Martian year of
388 Measurements. Geophysical Research Letters. doi:10.1002/2018GL077199.

389 Lee, C. O., et al. (2017), MAVEN observations of the solar cycle 24 space weather conditions at Mars,
390 J. Geophys. Res. Space Physics, 122, 2768–2794, doi: 10.1002/2016JA023495.

391 Lee, C. O., Jakosky, B. M., Luhmann, J. G., Brain, D. A., Mays, M. L., Hassler, D. M., et al. (2018).
392 Observations and impacts of the 10 September 2017 solar events at Mars: An overview and synthesis
393 of the initial results. *Geophysical Research Letters*, 45. https://doi.org/10.1029/2018GL079162

394 Lillis, R.J., Brain, D.A., Bougher, S.W. et al., Characterizing Atmospheric Escape from Mars Today and
395 Through Time, with MAVEN, Space Sci Rev (2015) 195 : 357. https://doi.org/10.1007/s11214-015-
396 0165-8

397 Luhmann, J. G., and J. U. Kozyra (1991), Dayside pickup oxygen ion precipitation at Venus and Mars:
398 Spatial distributions, energy deposition and consequences, *J. Geophys. Res.*, 96(A4), 5457–5467, doi:
399 10.1029/90JA01753.

400 Luhmann, J. G., R. E. Johnson, M. H. G. Zhang, Evolutionary impact of sputtering of the Martian
401 atmosphere by O^+ pickup ions, *Geophys. Res. Lett.*, 19, 2151–2154, 1992.
402 https://doi.org/10.1029/92GL02485

Lundin, R., S. Barabash, M. Holmström, H. Nilsson, Y. Futaana, R. Ramstad, M. Yamauchi, E. Dubinin, and M. Fraenz (2013), Solar cycle effects on the ion escape from Mars, *Geophys. Res. Lett.*, 40, 6028–6032, doi: 10.1002/2013GL058154.

Lundin, R., S. Barabash, M. Holmström, H. Nilsson, Y. Futaana, R. Ramstad, M. Yamauchi, E. Dubinin, and M. Fraenz (2013), Solar cycle effects on the ion escape from Mars, *Geophys. Res. Lett.*, 40, 6028–6032, doi: 10.1002/2013GL058154.

Ma, Y.-J., and A. F. Nagy (2007), Ion escape fluxes from Mars, *Geophys. Res. Lett.*, 34, L08201, doi: 10.1029/2006GL029208.

Martinez, A., Leblanc, F., Chaufray, J. Y., Modolo, R., Romanelli, N., Curry, S., et al (2019). Variability of precipitating ion fluxes during the September 2017 event at Mars. *Journal of Geophysical Research: Space Physics*, 124. https://doi.org/10.1029/2018JA026123

McFadden, J.P., Kortmann, O., Curtis, D. et al., MAVEN SupraThermal and Thermal Ion Composition (STATIC) Instrument, Space Sci Rev (2015) 195 : 199., https://doi.org/10.1007/s11214-015-0175-6

Modolo, R., et al. (2016), Mars-solar wind interaction: LatHyS, an improved parallel 3-D multispecies hybrid model, J. Geophys. Res. Space Physics, 121, 6378–6399, doi: 10.1002/2015JA022324.Ramstad,

Nilsson, H., G. Stenberg, S. Futaana, M. Holmstrom, S. Barabash, R. Lundin, N. Edberg, and A. Fedorov (2012), Ion distributions in the vicinity of Mars: Signatures of heating and acceleration processes, Earth Planets Space, 64(2), 135–148, doi:10.5047/eps.2011.04.011.

R., S. Barabash, Y. Futaana, H. Nilsson, X.-D. Wang, and M. Holmström (2015), The Martian atmospheric ion escape rate dependence on solar wind and solar EUV conditions: 1. Seven years of Mars Express observations, *J. Geophys. Res. Planets*, 120, 1298–1309, doi: 10.1002/2015JE004816.

Ramstad, R., S. Barabash, F. Yoshifumi, and M. Holmström (2017), Solar wind- and EUV-dependent models for the shapes of the Martian plasma boundaries based on Mars Express measurements, *J. Geophys. Res. Space Physics*, 122, 7279–7290, doi:10.1002/2017JA024098.

Ronan Modolo, Gérard M. Chanteur, E. Dubinin, A. P. Matthews. Influence of the solar EUV flux on the Martian plasma environment. Annales Geophysicae, European Geosciences Union, 2005, 23 (2), pp.433-444. <hal-00329361>

Terada, N., Y. N. Kulikov, H. Lammer, H. I. M. Lichtenegger, T. Tanaka, H. Shinagawa, and T. Zhang (2009), Atmosphere and water loss from early Mars under extreme solar wind and extreme ultraviolet conditions, *Astrobiology*, 9(1), 55–70, doi:10.1089/ast.2008.0250.

Wang, Y.-C., J. G. Luhmann, F. Leblanc, X. Fang, R. E. Johnson, Y. Ma, W.-H. Ip, and L. Li (2014), Modeling of the O^+ pickup ion sputtering efficiency dependence on solar wind conditions for the Martian atmosphere, *J. Geophys. Res. Planets*, 119, 93–108, doi: 10.1002/2013JE004413.

Wang, Y.-C., J. G. Luhmann, X. Fang, F. Leblanc, R. E. Johnson, Y. Ma, and W.-H. Ip (2015), Statistical studies on Mars atmospheric sputtering by precipitating pickup O^+: Preparation for the MAVEN mission, *J. Geophys. Res. Planets*, 120, 34–50, doi: 10.1002/2014JE004660.

Xu S. et al., (2018), Investigation of Martian magnetic topology response to 2017 September ICME, *Geophys. Res. Lett.*, 45, doi: 10.1029/2018GL077708.

Figure1.

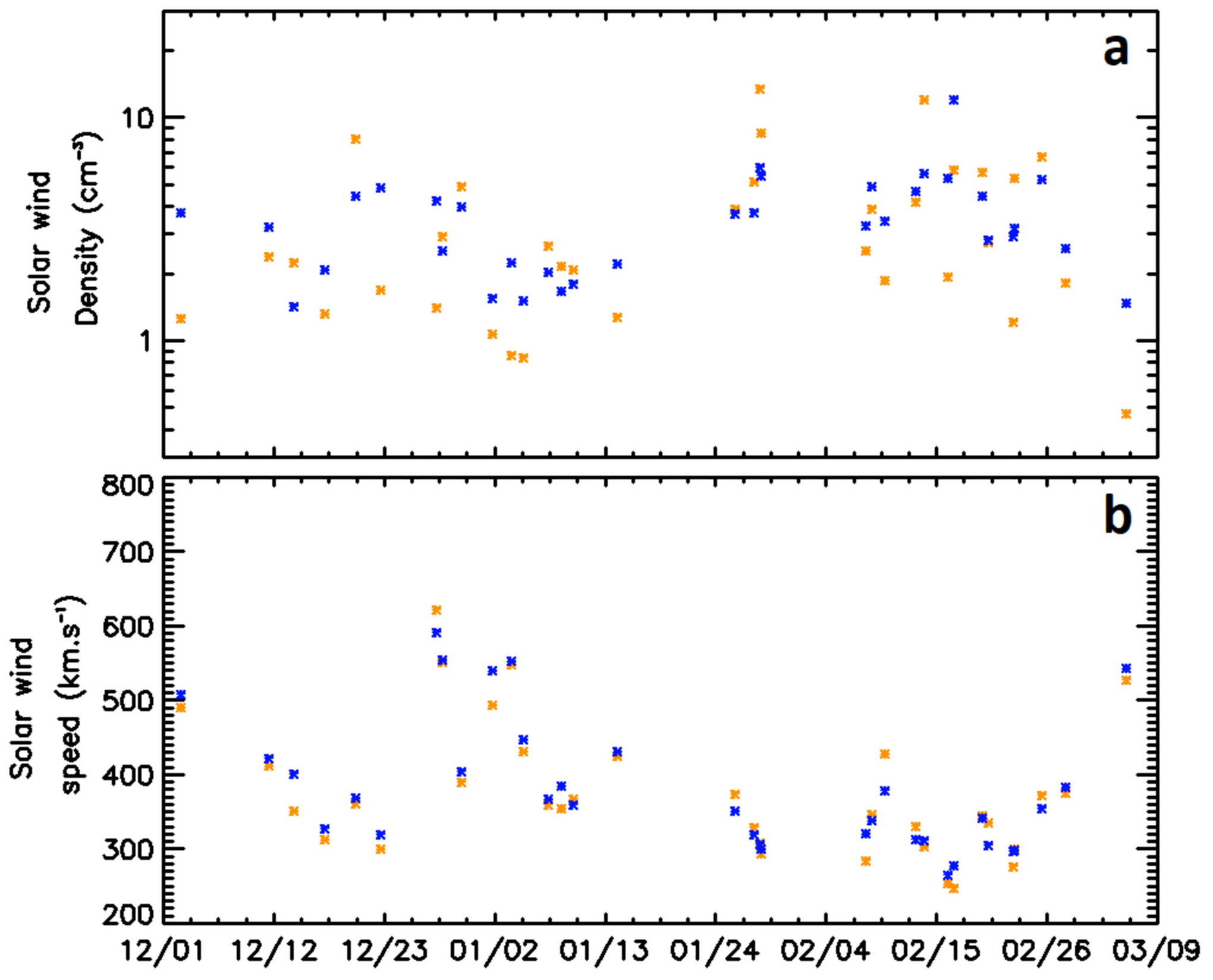
a
Solar wind
Density (cm⁻³)
10
1
b
Solar wind
speed (km.s⁻¹)
800
700
600
500
400
300
200
12/01
12/12
12/23
01/02
01/13
01/24
02/04
02/15
02/26
03/09

Figure2.

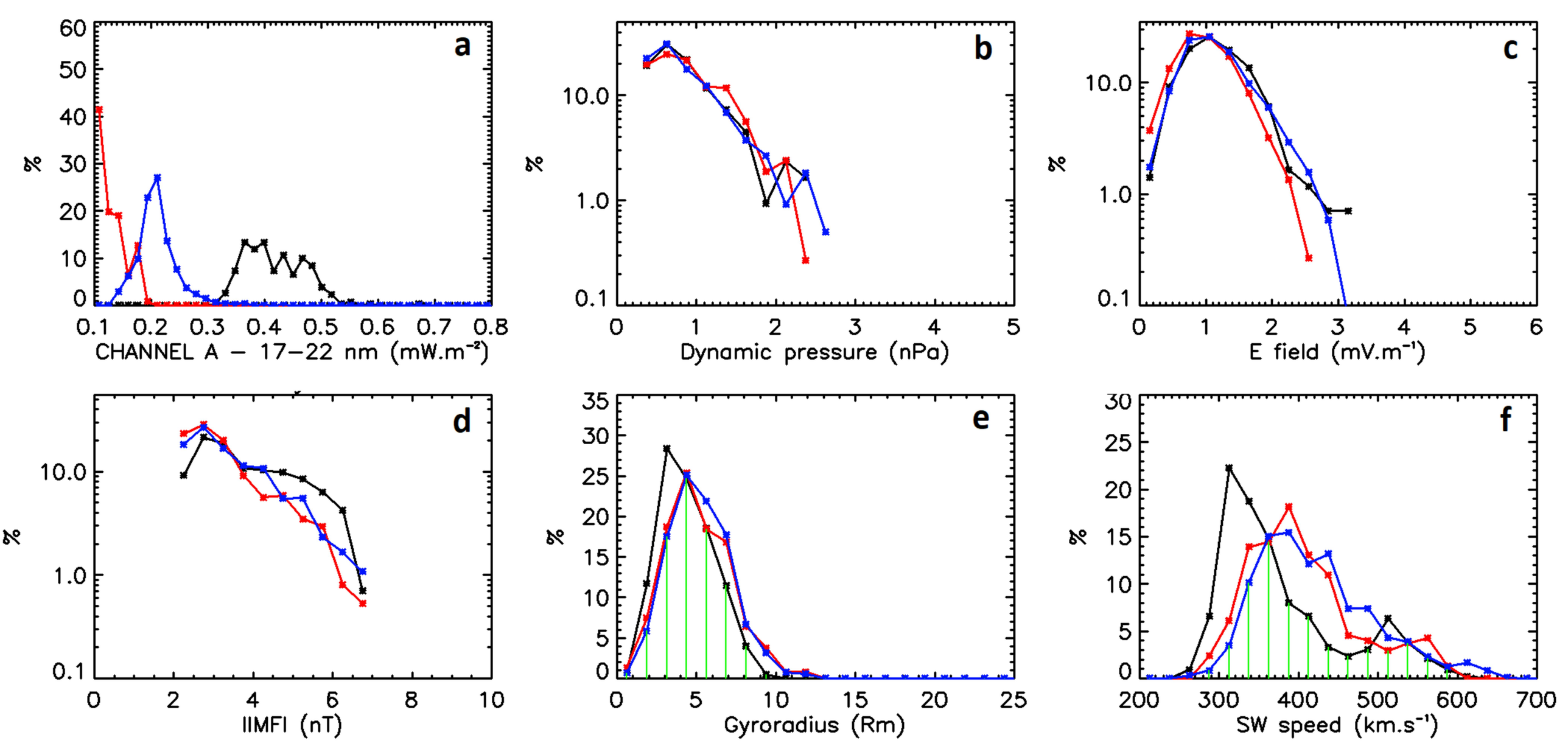
a
%
CHANNEL A – 17–22 nm (mW.m⁻²)
b
%
Dynamic pressure (nPa)
c
%
E field (mV.m⁻¹)
d
%
IIMFI (nT)
e
%
Gyroradius (Rm)
f
%
SW speed (km.s⁻¹)

Figure3.

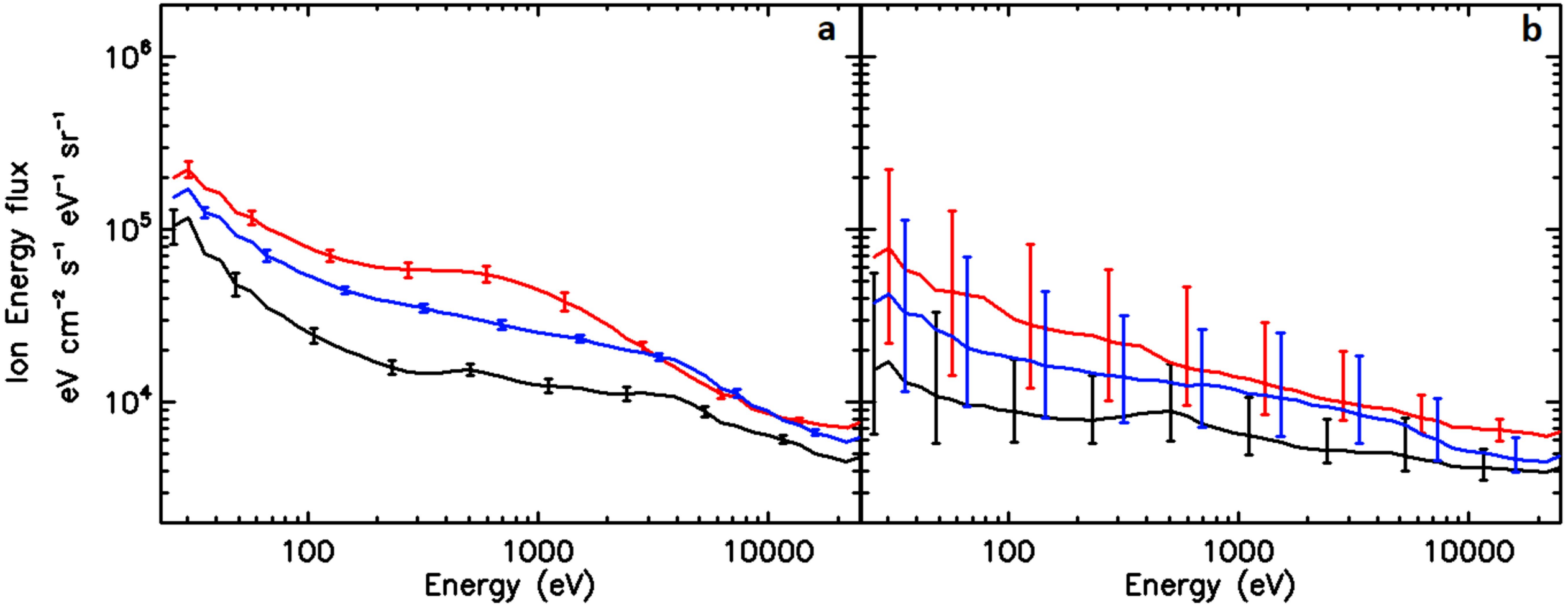
a
b
Ion Energy flux
eV cm^{-2} s^{-1} eV^{-1} sr^{-1}
10^6
10^5
10^4
100
1000
10000
Energy (eV)
100
1000
10000
Energy (eV)